A universal Strouhal-Reynolds-Froude-number relationship for trailing vortices in a laminar free-surface flow

Tong Chen and Allen T. Chwang
Department of Mechanical Engineering, The University of Hong Kong
Pokfulam Road, Hong Kong

Abstract

Two-dimensional numerical simulations are carried out in the present paper to investigate the vortex-shedding features in the wake of a fully-submerged hydrofoil translating with a positive angle of attack beneath a free surface. The present numerical method is a finite element projection procedure, which can tackle realistic configurations and easily implement the fully-nonlinear free-surface boundary conditions. Extensive numerical experiments provide details of the trailing vortices in a laminar free-surface flow. Through parametric studies of the computational results, a universal and continuous Strouhal-Reynolds-Froude-number relationship is proposed. Various interesting and unique characteristics of the trailing vortices under the influence of a free surface are found and discussed in detail.

1. Introduction

The transformation between kinetic and potential energies and the coexistence of viscous, gravity and surface-tension forces at an unknown wavy boundary make the free-surface phenomena difficult to study. Wave signatures are known to be caused by the interaction between the vortex-induced wake behind a moving object and a deformable air-water interface, responsible for some interesting vortex behaviors, such as the vortex rebounding, rollers at wave crests, creation of secondary eddies with mass and momentum transport, straight and sharp surface depression labeled as scars and striations, and the wave resonance due to jet attachment to the free surface (Sheridan *et al.*, 1997). A better understanding of these flow behaviors is fundamental to ocean engineering and undersea technology. However, the physics of flow structures and the free-surface interaction, especially the Kármán vortex street beneath a free surface, remains elusive due to the complexity in devising and using mathematical formulations, numerical schemes and physical experiments (Sarpkaya, 1996). Available experiments have shown that the trailing vortices can become inherently unstable to centrifugal and helical disturbances and to the existence of a wake-like or jet-like velocity profile. The primary vortices may also rebound due to shear and small eddies at the free surface (Ohring & Lugt, 1991). Recently, Zhang *et al.* (1999) investigated the mechanism of vortex connection near a free surface in a three-dimensional numerical wave tank. They confirmed the viscous and blockage double sublayers beneath the free surface. Their numerical method was further extended by Shen *et al.* (1999) to directly simulate the surface-layer formation in free-surface turbulent flows. Systematic computations indicated that the blockage layer results from the kinematic boundary condition at the free surface, and the viscous surface layer is caused by the dynamic stress-free conditions. By visualizing the wakes of a flow past a cylinder close to the free surface, Sheridan *et al.* (1997) experimentally studied the wake instability, the Froude-number effect, the free-surface distortion, and the vorticity flux from the free surface and the cylinder surface. They conjectured that the localized separation or complete separation from the free surface is responsible for the generation of a vorticity layer from the free surface.

There exists a similarity of trailing-wake structures in flows between a body close to a wall and a fully-submerged body adjacent to a free surface. In terms of blockage, a free surface is indeed a material boundary. Nevertheless, the curvature of, and the free traction at, the free surface make the latter scenario even more complicated. The central interest of the present work lies in the study of the generation of trailing vortices in the wake of a fully submerged hydrofoil. By monitoring the alternation behaviors of a trailing wake, the free-surface effect on the flow structure is systematically examined in the numerical experiments, involving substantial combinations of Reynolds and Froude numbers. This parametric study reveals some very unique and interesting features of the trailing vortices in the presence of a free surface.

2. Description of the flow problem

Let us consider a fully submerged hydrofoil in a uniform flow, and focus on the free-surface influence on the entire flow structure, particularly on the trailing vortices. In a two-dimensional Cartesian reference frame $\mathbf{x} = (x, y)$ with x-axis in the uniform flow direction on the mean free surface and the y-axis pointing vertically upward, the incompressible Navier-Stokes and continuity equations are

$$\mathbf{u}_t + (\mathbf{u}\cdot\nabla)\mathbf{u} = -\nabla P + Re^{-1}\nabla^2\mathbf{u}, \qquad (1)$$

$$\nabla \cdot \mathbf{u} = 0, \tag{2}$$

where the hydrodynamic pressure $P = p + y/Fr^2$ is the total pressure p minus the hydrostatic pressure, $\mathbf{u} = (u, v)$ is the velocity and t is the time.

$$Fr = U_0/(gL)^{1/2} \text{ and } Re = \rho U_0 L/\mu_0$$

are the Froude and Reynolds numbers respectively, based on a characteristic length L, a reference velocity U_0, the molecular viscosity μ_0, the gravitational constant g and the fluid density ρ. p is non-dimensionalized by ρU_0^2.

The governing equations are to be solved subject to the following boundary conditions: (a) essential Dirichlet type of specified velocity on solid surfaces (no-slip) and inlet (incident free-stream) Γ_1 and (b) natural Neumann type of prescribed traction vector at open boundaries (traction free) Γ_2 truncated far enough from the region concerned and at a time-dependent free surface Γ_3 defined by $y = h(x, t)$,

$$\mathbf{u}|_{\Gamma_1} = \mathbf{b}, \tag{3}$$

$$(-p\mathbf{I} + \sigma) \cdot \mathbf{n}|_{\Gamma_2+\Gamma_3} = \mathbf{c}. \tag{4}$$

Here, $\sigma = Re^{-1}[\nabla \mathbf{u} + (\nabla \mathbf{u})^T]$ is the deviatoric stress, $\mathbf{I}$ is the identity tensor, superscript "T" denotes the transposed tensor and h is the free-surface elevation. $\mathbf{n} = (n_x, n_y)$ is the outward unit vectors normal to the surfaces. The fact that no fluid particle leaves the free surface provides additionally the kinematic boundary condition

$$h_t + uh_x = v \qquad \text{on } \Gamma_3. \tag{5}$$

Meanwhile, the traction is no longer free if the external free-surface tension q is appreciable: $\mathbf{c} = q\mathbf{n}$. Assuming that q is proportional to the interface curvature

$$\kappa = h_{xx}(1 + h_x^2)^{-3/2},$$

we have

$$q = We^{-1}\kappa,$$

where $We = \rho U_0^2 L/\gamma$ is the Weber number, γ being the coefficient of surface tension. Dynamic condition (4) at Γ_3 also implies the relation ($u_n = \mathbf{u} \cdot \mathbf{n}$)

$$(p+q)|_{\Gamma_3} = \frac{2}{Re}\frac{\partial u_n}{\partial n}. \tag{6}$$

3. Numerical method

Using the second-order Crank-Nicolson time integration, the projection finite element procedure turns equations (1) and (2) into an uncoupled system of equations as

$$\mathbf{M}\mathbf{u}^* = \mathbf{M}\mathbf{u}^n - \tilde{\mathbf{G}}\Phi^n - \Delta t[(\mathbf{C} + Re^{-1}\mathbf{K})\mathbf{u} - \mathbf{F}]^{n+1/2}, \tag{7}$$

$$\mathbf{K}\Phi^{n+1} = \tilde{\mathbf{G}}^T \cdot \mathbf{u}^* + \mathbf{B}, \tag{8}$$

$$\mathbf{u}^{n+1} = \mathbf{u}^* - \mathbf{M}^{-1}\tilde{\mathbf{G}}\Phi^{n+1}, \tag{9}$$

where $\Phi = \Delta t P / 2$ and $\mathbf{u}^*$ is an intermediate velocity. Superscripts "$n+1$" and "n" refer to the current and previous time levels, Δt is the time increment, superscript "e" denotes the averaged values taken at element centroids and the coefficient matrices are

$$\mathbf{M} = \int_\Omega \Psi\Psi^T d\Omega, \quad \tilde{\mathbf{G}} = \int_\Omega \Psi\nabla\Psi^T d\Omega,$$

$$\mathbf{K} = \int_\Omega \nabla\Psi \cdot \nabla\Psi^T d\Omega, \quad \mathbf{C} = (\mathbf{u} - \mathbf{u}^g)^e \cdot \tilde{\mathbf{G}}.$$

$\mathbf{K}$ is the Laplacian matrix and $\tilde{\mathbf{G}}$ the gradient matrices. The nonlinear convective matrix $\mathbf{C}$ has been modified to incorporate the mesh velocity

$$\mathbf{u}^g = (\mathbf{x}^{n+1} - \mathbf{x}^n)/\Delta t$$

since the mesh has to be adaptive to the change of topology. To keep the procedure efficient, the consistent mass matrix $\mathbf{M}$ is lumped onto the diagonals and penalized to impose the essential boundary condition (3). Equations (7) and (8) are weak formulations contain boundary integrals $\mathbf{F}$ and $\mathbf{B}$ by which the free-surface viscous and capillary effects are incorporated as

$$\mathbf{F} = \int_{\Gamma_2+\Gamma_3} \frac{1}{Re}\frac{\partial \mathbf{u}}{\partial n}\Psi d\Gamma,$$

$$\mathbf{B} = \int_{\Gamma_1+\Gamma_2} (\nabla\Phi - \mathbf{u}^*) \cdot \mathbf{n}\Psi d\Gamma = -\int_{\Gamma_1+\Gamma_2} \mathbf{u}^{n+1} \cdot \mathbf{n}\Psi d\Gamma.$$

Equation (8) is also subject to the Dirichlet-type dynamic free surface constraint from (6),

$$\Phi|_{\Gamma_3} = \frac{\Delta t}{2}\left(\frac{h}{Fr^2} - \frac{\kappa}{We} + \frac{2}{Re}\frac{\partial u_n}{\partial n}\right). \tag{10}$$

The data structure and solution strategy follow from Chen (1999). Fully nonlinear kinematic boundary condition (5) is implemented to update the free surface in a time-marching manner. To keep the global second-order accuracy in time, the Crank-Nicolson finite difference scheme is adopted while the convective term is treated with the third-order upwind scheme. Artificial damping is used at the up/downstream open boundaries for outgoing waves. Details of the free-surface updating scheme and the mesh adaptation were described by Chen & Chwang (2000a).

4. Numerical experiments

The present numerical formulation was validated by comparing its results with experimental measurements of Duncan (1983) for a fully submerged NACA0012 hydrofoil with chord length L in a uniform flow (Chen & Chwang, 2000b). The depth of submergence s =1.034 is measured at the mid-chord and the angle of attack is $\theta = 5°$. No bottom effect is considered. The coefficient of free-surface tension is fixed at We =

1,784 for all the cases. Figure 1 shows the computational domain x (–6.5, 10.0) and y (–4.0, h), and the mesh division. The grid efficiency of an unstructured mesh is obvious. The time increment is Δt = 0.002. To be more representative of the flow physics, the submergence-based Froude number $Fr = U_0/(gs)^{1/2}$ is hereinafter adopted.

Figures 2(a, b, c, d) show respectively the instantaneous contours of velocity components (u, v), hydrodynamic pressure P and vorticity ω for the case indicated in the figure caption. The vorticity with strength $|\omega| \geq 0.5$ is flooded with light and dark colours for negative and positive vortices (ω^-, ω^+) respectively. For moderately high Reynolds number laminar flows, the Kármán vortex street demonstrates periodical alternation with respect to the mean flow direction in a quasi-steady manner. The whirled low pressure spots locate the vortex centres.

The free-surface effect on the trailing vortices is studied by analyzing the dependence of the frequency at which vortices are shed in a Kármán vortex street on both the viscous and gravity effects. Velocity signals shown in Figure 3 are recorded at a typical near-wake sampling point 1.5L downstream of the trailing edge. A large number of cases is computed and the Strouhal numbers ($St = f_s L/U_0$) are obtained by spectral analysis using the Fourier Transformation of the wake velocity fluctuations (frequency accuracy Δf = 0.01, time integration interval t = 12.0 ~ 26.0). Predominant vortex-shedding Strouhal frequencies are detected with their harmonics in the spectra. The Strouhal number increases with the Reynolds number and matches very well the *St-Re* relationship suggested by Williamson (1988) based on experiments of laminar flows past a circular cylinder without a free surface,

$$St = A_1 / Re + A_2 + A_3 Re\,. \qquad (11)$$

However, the original coefficients A_1 = –3.3265, A_2 = 0.1816 and $A_3 = 1.6\times10^{-4}$ need to be modified due to the change of geometry, and are apparently functions of Froude number in the present free-surface flow. After data analysis, we propose a universal and continuous *St-Re-Fr* relationship for the laminar vortex shedding behind a NACA0012 hydrofoil in a free-surface flow, in which A_i (i = 1~3) are revised empirically by

$$A_i = B_i \exp(\beta Fr^{\alpha}) + C_i \exp(\beta Fr^{-\alpha}), \qquad (12)$$

with α = 6 and β = –0.052. Regression by the least squares method produces coefficients B_i and C_i as tabulated in Table 1. Figures 4 (a, b) compare the proposed formula with the computational data for isolated Froude and Reynolds numbers, respectively. The relative mean accuracy of formulae (11) and (12) is

$$\varepsilon = [\,\Sigma\,(St - St_{\text{comput}})^2 / \Sigma St^2\,]^{1/2} = 4.5\times10^{-3}$$

for all the computations. It is worth to mention that formulae (11) and (12) are only valid for purely laminar flows and no breaking waves on the free surface.

Table 1. Coefficients B_i and C_i for a NACA0012 hydrofoil in a free-surface flow

i	1	2	3
B_i	–1688.142	1.986	2.886×10^{-5}
C_i	–2336.763	0.855	-4.507×10^{-6}

The dependence of A_i on Froude number strongly exhibits the correlation of the viscosity and gravity in the shed trailing vortices. It is of particular interest to note from Fig. 4a that the *St-Re* curves cross each other at a critical Reynolds number ($Re \cong 2850$). Via extrapolation, one may also obtain the minimum Reynolds number at which the regular Kármán vortex street can be observed ($Re \cong$ 850, 1000 and 1100 for Fr = 0.0, 0.5578 and 0.6097 respectively with St = 0.0). This explains a very important scenario of the free-surface flow that a higher Froude number will result in a later onset of vortex shedding. This conjecture is strongly supported by the experiments of Sheridan *et al.* (1995). They found that the presence of a free surface allows small-scale Kelvin-Helmholtz instabilities to occur, but inhibits the onset of Kármán instability. However, once the Kármán instability has been triggered and Reynolds number has exceeded this critical value, it is clearly shown that a higher Froude number will always lead to a faster vortex-shedding frequency in laminar flows.

In addition, remarks can be drawn readily from the *St-Fr* curves in Fig. 4b about the Froude number effect on the shedding frequency. The Strouhal number decays following roughly a power law by an index larger than 6.0 when $Fr \leq 0.45$. Therefore, as far as the vortex alternation is concerned, the free-surface effect can virtually be ignored for all Reynolds numbers with $Fr \leq 0.45$. For $0.5 \leq Fr \leq 0.75$, the Strouhal number is almost linearly proportional to the Froude number. By dropping the first term in (12), the slope k can be roughly calculated from (11) and (12) as

$$k \cong C(1+\alpha)\exp(-1/\alpha - 1) / Fr^{*} \cong 3.66C, \qquad (13)$$

where

$$C(Re) = C_1 / Re + C_2 + C_3 Re\,, \qquad (14)$$

and Fr^{*} denotes the turning point of the *St-Fr* curves at which the second derivative vanishes,

$$Fr^{*} = \left(\frac{-\alpha\beta}{1+\alpha}\right)^{\frac{1}{\alpha}} \cong 0.5954\,. \qquad (15)$$

The tangent lines are shown in Fig. 4b by the dotted lines for relevant Reynolds numbers. It is noted that k increases slightly with increasing Reynolds number but is independent of Froude number. Equation (12) indicates that as $Fr \to \infty$ yet the flow remains laminar and no wave breaking (though these requirements can hardly be met in the present problem), the free-surface effect will also disappear. The present formulae also imply that after the Froude number exceeds a threshold value, the Strouhal number starts to decrease as

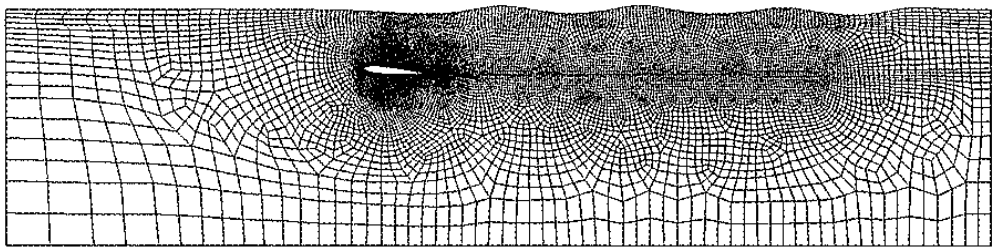

Figure 1. Computational domain and mesh division (total nodes=15,324, total element = 15,076, free-surface nodes = 209 and body-surface elements = 184)

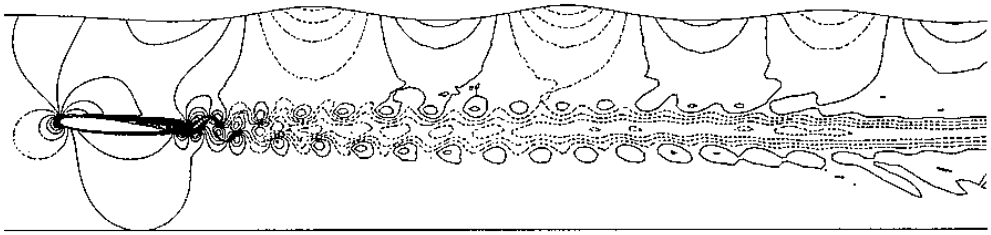

(a) u: (u_{min}=–0.25, u_{max}=1.33, Δu=0.053, solid lines u>1, dotted lines u≤1)

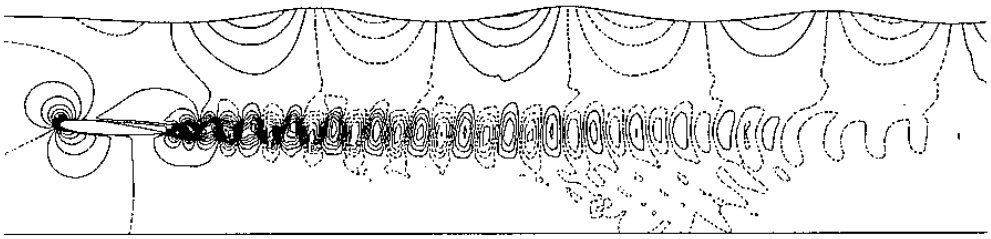

(b) v: (v_{min}=–0.53, v_{max}=0.82, Δv=0.045, solid lines v>0, dotted lines v≤0)

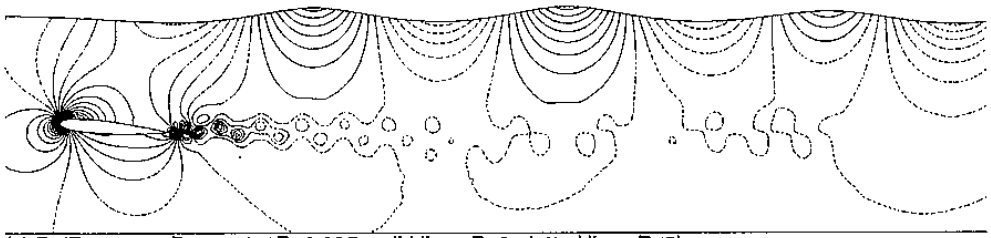

(c) P: (P_{min}=–0.5, P_{max}=0.5, ΔP=0.025, solid lines P>0, dotted lines P≤0)

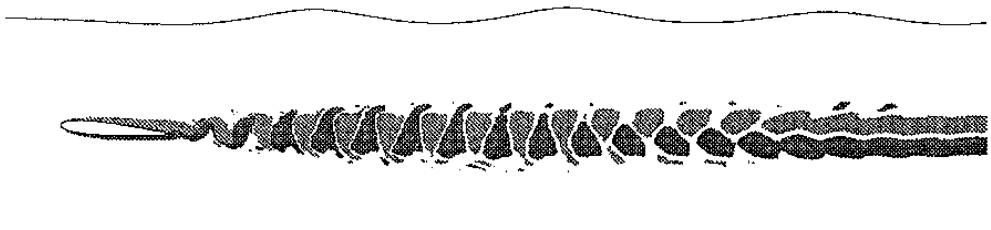

(d) ω: (colour: ω^- = light, ω^+ = dark, $|\omega| \geq 0.5$)

Figure 2. Instantaneous field variable contours at t=25.0, Re=1×10^4, Fr=0.6097, We=1,784

expected, and converges to a new level lower than that for the $Fr = 0$ case,

$$St_{Fr=\infty} = C(Re) < B(Re) = St_{Fr=0}.$$

5. Conclusions

The present numerical experiments have preliminarily revealed some interesting and unique effect of the free surface on the trailing vortex shedding. A universal and continuous *St-Re-Fr* relationship for the laminar vortex shedding in a free-surface flow is proposed based on computations. It is found that the presence of a free surface allows small-scale Kelvin-Helmholtz instabilities to occur, but inhibits the onset of Kármán instability. However, once the Kármán instability has been excited and the Reynolds number exceeds a critical value, a higher Froude number will always lead to a higher vortex-shedding frequency in laminar flows.

ACKNOWLEDGEMENTS

This research was sponsored by the Hong Kong Research Grants Council under Grants HKU 7066/97E and NSFC/HKU 8.

REFERENCES

Chen, T (1999), "Numerical computations on free-surface flow", *Ph.D. Thesis*, The University of Hong Kong.

Chen, T & Chwang, AT (2000a), "Calculations of nonlinear waves generated by complex body motion". *J. Mech. Eng. Sci.* Proc. part C (in press).

Chen, T & Chwang, AT (2000b), "Effect of free-surface on laminar flow past arbitrary bodies". *Proc 4th Int'l Conference on Hydrodynamics*, Yokohama, Japan (in press).

Duncan, JH (1983), "The breaking and non-breaking wave resistance of a two-dimensional hydrofoil". *J. Fluid Mech.* **126**, 507-520.

Ohring, S & Lugt, HJ (1991), "Interaction of a viscous vortex pair with a free surface". *J. Fluid Mech.* **227**, 47-70.

Sarpkaya, T (1996), "Vorticity, free surface and surfactants". *Annu. Rev. Fluid Mech.* **28**, 83-128.

Shen, L, Zhang, X, Yue, DKP & Triantafyllon, GS (1999), "The surface layer for free-surface turbulent flows". *J. Fluid Mech.* **386**, 167-212.

Sheridan, J, Lin, J-C & Rockwell, D (1997), "Flow past a cylinder close to a free surface". *J. Fluid Mech.* **330**, 1-3.

Williamson, CHK (1988), "Defining a universal and continuous Strouhal-Reynolds number relationship for the laminar vortex shedding of a circular cylinder". *Phys. Fluids* **31**, 2742-2744.

Zhang, C, Shen, L & Yue, DKP (1999), "The mechanism of vortex connection at a free-surface". *J. Fluid Mech.* **384**, 207-241.

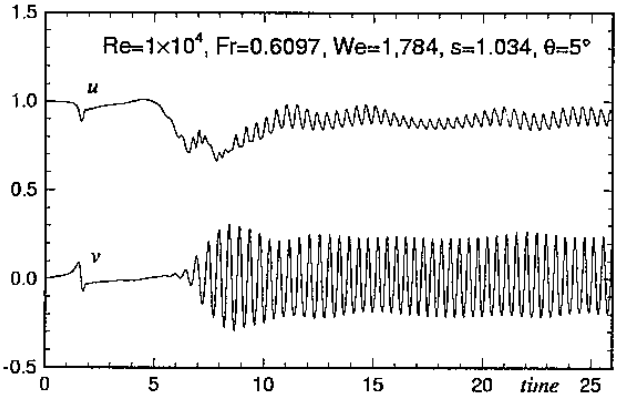

Figure 3. Velocity siganls recorded at a sampling point 1.5L downstream of the trailing edge

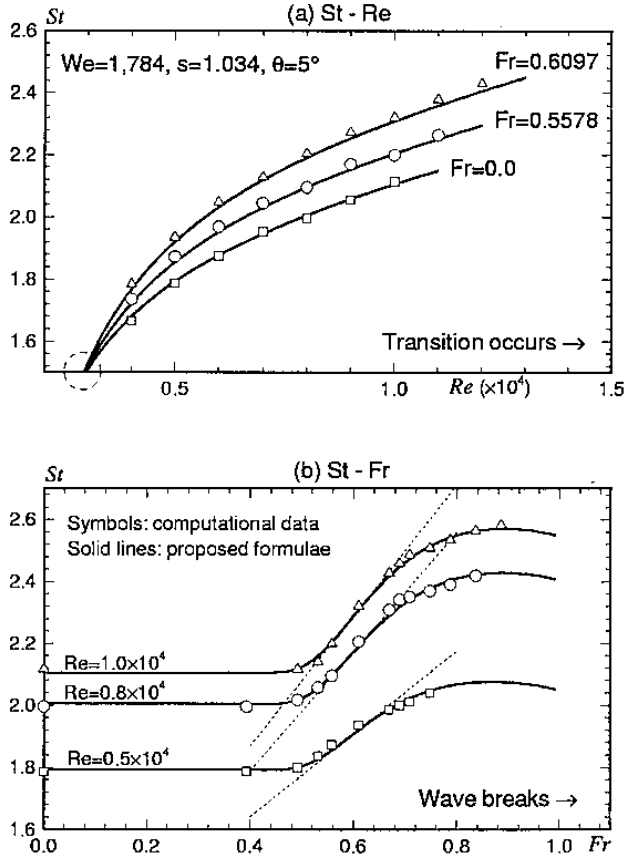

Figure 4. St-Re-Fr relationship for the vortex shedding behind a NACA0012 hydrofoil in a free-surface laminar flow